Impact of heating and cooling loads on battery energy storage system sizing in extreme cold climates

Walker Olis [*], David Rosewater, Tu Nguyen, Raymond H. Byrne

Sandia National Laboratories, Albuquerque, NM 87185, USA

ARTICLE INFO

ABSTRACT

Efficient operation of battery energy storage systems requires that battery temperature remains within a specific range. Current techno-economic models neglect the parasitic loads heating and cooling operations have on these devices, assuming they operate at constant temperature. In this work, these effects are investigated considering the optimal sizing of battery energy storage systems when deployed in cold environments. A peak shaving application is presented as a linear programming problem which is then formulated in the PYOMO optimization programming language. The building energy simulation software EnergyPlus is used to model the heating, ventilation, and air conditioning load of the battery energy storage system enclosure. Case studies are conducted for eight locations in the United States considering a nickel manganese cobalt oxide lithium ion battery type and whether the power conversion system is inside or outside the enclosure. The results show an increase of 42% to 300% in energy capacity size, 43% to 217% in power rating, and 43% to 296% increase in capital cost dependent on location. This analysis shows that the heating, ventilation, and air conditioning load can have a large impact on the optimal sizes and cost of a battery energy storage system and merit consideration in techno-economic studies.

1. Introduction

Energy storage is one of the technologies driving current transformation of the electric power grid toward a smarter, more reliable, and more resilient future grid [1]. Reducing consumption of fossil fuels requires increased integration of renewable generation which becomes more reliable when paired with energy storage due to their intermittency [2]. The versatility of energy storage systems (ESSs) adds flexibility to the electric grid in the face of distributed generation [3]. ESSs can provide a range of services from grid level applications, such as energy arbitrage and frequency regulation, to individual customer support by providing back-up power generation, renewable generation firming, and peak shaving [4]. Optimal sizing of these devices remains challenging because of technology characteristics, location, and expected lifetime. Current techno-economic battery energy storage system (BESS) models neglect the effects of battery and enclosure thermal management.

Sizing ESSs in techno-economic studies is widely researched. Optimal sizing of BESSs with a photo-voltaic (PV) plant is presented in [5] to maximize revenue of the PV-BESS pair. In [6], PV-BESS size, operation, and energy management is optimized to generate revenue with consideration of the capacity of grid connection. A multi-objective optimization framework was developed in [7] to size ESSs considering peak shaving, PV utilization, and ESS cost. A Pareto front is obtained to compare the value of ESS cost with both reducing the demand charge and improving PV utilization. A Discrete Fourier Transform (DFT) approach is proposed in [8] to size a hybrid ESS containing battery energy storage and pumped hydropower to mitigate wind power fluctuations. In [9] a comprehensive study was performed on the optimal size, technology, and depth of discharge of battery energy storage to reduce the microgrid operational cost and improve reliability. This work builds on the results in [10] to improve the expected lifetime of a BESS and analyze the effects of microgrid participation in energy markets.

A comparison between stand alone and grid supplemented PV with BESS is investigated in [11] with respect to optimal sizing and energy management of the system. The main findings are grid supplemented systems provide lower costs at the expense of higher life cycle emissions. In [12], optimal sizing of a hybrid concentrated solar photovoltaic (CSP), PV, and wind system supplemented with BESS and thermal energy storage (TES). The electric system cascade extended analysis is developed to determine optimal system configuration based upon the loss of power supply probability (LPSP) and the levelized cost of electricity (LCOE). A techno-economic analysis of a solar PV and direct current BESS in a community sharing scenario is analyzed in [13],

---

Nomenclature

τ	Length of time step (e.g. one hour)
i	Time step
m	Time period (e.g month)
A	Set of time steps in optimization
M	Set of time periods in optimization
$\mathbf{A}_m$	Subset of time steps in **A**
q_i^c	Energy charged in time step i {kWh}
q_i^d	Energy discharged in time step i {kWh}
q_i^{grid}	Excess energy bought from grid in time step i {kWh}
q_i^{load}	Load energy in time step i {kWh}
q_i^{hvac}	HVAC load energy in time step i {kWh}
Q	Maximum battery energy transfer {kWh}
$\bar{p}$	ESS power rating {kW}
$\bar{S}$	ESS energy capacity {kWh}
S	State of Energy {kWh}
S_{max}	Maximum SOC {kWh}
S_{min}	Minimum SOC {kWh}
n^s	Self discharge efficiency
n^{rt}	Round trip efficiency
C^{ESS}	Total cost of energy storage system {\$}
C^E	Total energy bill {\$}
c^p	Cost of ESS per kW {$\frac{\$}{\text{kW}}$}
c^q	Cost of ESS per kWh {$\frac{\$}{\text{kWh}}$}
c^d	Demand charge {$\frac{\$}{\text{kW}}$}
c^e	Cost of energy {$\frac{\$}{\text{kWh}}$}
AKA	Anchorage, AK
AKF	Fairbanks, AK
CO	Leadville, CO
MA	Boston, MA
MN	Minneapolis, MN
MT	Butte, MT
ND	Bismarck, ND
NY	Buffalo, NY
ESS	Energy Storage System
BESS	Battery Energy Storage System
LP	Linear Program
HVAC	Heating, Ventilation, and Air Conditioning
PCS	Power Conversion System
NMC	Nickel Manganese Cobalt Oxide
ERM	Energy Reservoir Model
SOC	State of Charge
PTAC	Packaged Terminal Air Conditioner

maximizing the energy generation and penetration while minimizing costs at the optimal size.

The joint placement and size of wind turbines and BESSs is investigated in [14] particularly considering the reactive power support the BESS can provide for the system. The proposed optimization improved voltage profiles of load buses, reduced active and reactive power losses, and reduced costs in a 36 bus distribution system. In [15], a two layer optimization approach is proposed to optimally size a BESS considering a virtual energy storage system as an air conditioned home and high PV penetration in a smart microgrid. In the first layer an initial BESS size is determined based upon the VESS participation, then the second layer determines the optimal BESS size considering system constraints. A dynamic programming method is used to obtain the optimal size of BESS

in a wind turbine BESS system in [16]. The authors compared a rules-based method, genetic algorithm, a dynamic programming method considering degradation, and a dynamic programming method without degradation and are able to show the dynamic programming method considering degradation reduces costs by extending the lifespan of the BESS and reducing operating costs of the wind plant.

In [17], a multi-stage framework is developed to optimally size and operate a hybrid electrical–thermal storage system. Case studies show that the hybrid system is more reliable and cost-effective than a stand alone storage system of either type and the multi-stage framework lowers overall costs of the system compared to a rules based approach. A two-step cost based method is used in [18] to optimally size a BESS in a micro-grid and is shown to reduce costs compared to the particle swarm algorithm and genetic algorithm. The authors in [19] proposes the improved cayote optimization algorithm to optimally size and locate BESS to reduce power losses in the distribution grid and is shown to improve the efficiency when compared to the firefly algorithm, whale optimization algorithm, and particle swarm optimization.

None of the aforementioned techno-economic studies consider the parasitic losses associated with heating and cooling loads of the ESS enclosure. In particular, BESS must be kept within an operating temperature range to ensure optimal performance and in many cases maintain the warranty. Control models often consider heating and cooling of the device when it can affect battery operation. The work in [20] presents a two stage optimal control strategy for a BESS in a microgrid considering the battery temperature. The first stage determines the optimal battery and fan operations to manage the battery temperature within thermal limits, while the second optimizes the microgrid operation. The thermal model includes internal resistive heating with conductive and convective cooling terms for each battery cell. This strategy is shown to keep the battery temperature within thermal limits at a slightly higher operational cost.

An equivalent circuit model considering thermal effects for Vanadium Redox Flow (VRB) BESSs is developed in [21] using a third order Cauer network for the thermal circuit. The model is experimentally validated with a 5kW/3kWh system and then used in a simulation supporting a wind power plant. In [22] an electrothermal coupling model is developed considering battery aging for electric vehicles. A nonlinear model predictive control (NMPC) heating optimization strategy is proposed using this electrothermal model at low temperatures. Simulation results show an improvement in both heating time and energy consumption when this method is compared to using an electric heater. A thermoelectric coupled model specific to lithium-ion batteries is developed in [23] for an NMPC optimal charging method suitable for the temperature range −5° to 45 °C. This model is shown to reduce energy loss and temperature rise during a similar charging time period when compared with a constant current charging method. A comparative study of control-oriented thermal models for lithium-ion batteries in vehicle and grid applications is presented in [24]. The models are evaluated in situations where both core and surface temperature are known and also where only the surface temperature is known using simulations and experimental data sets of lithium iron phosphate batteries. The polynomial approximation is found to be the best model in practical applications when considering model assumptions, model fidelity, computational cost, and model sensitivity. In [25], a comprehensive review of optimal battery control strategies is presented. Section 4 in [25] describes temperature modeling and shows that optimal control of the battery and heating, ventilation, and air conditioning (HVAC) unit setpoints provide an electricity bill reduction while keeping the battery temperature within operating range.

The objective of this paper is to offer a techno-economic sizing method which considers the parasitic loads due to HVAC operation. The proposed method calculates the optimal size of a BESS in techno-economic studies based on the application, battery type, and local climate. This method is coded in python and uses the PYOMO optimization programming language [26,27] and the building energy simulation

software EnergyPlus [28,29]. Eight locations are considered and the objective is to identify the system size that meets the performance requirements and reduces capital and operational costs. Optimization of the capital costs of a BESS and energy bill is formulated as a Linear Programming (LP) problem for peak shaving using a linear energy reservoir model (ERM). An EnergyPlus model is created to determine the electric load due to heating and cooling the BESS enclosure using a non-linear ERM, which is then incorporated into the optimization framework. This offers an improvement to the techno-economic studies discussed, which do no consider the parasitic loads due to HVAC operation. The specific contributions of this paper are (1) a new energy storage sizing algorithm that performs better than current models in extreme climates, and (2) a quantitative estimate of the cost savings achievable in different locations by including the power conversion system (PCS) inside the battery enclosure to reduce net heating load.

The paper is organized as follows. Section 2 presents the algorithm structure along with the optimization formulation. Section 3 discusses the results of each scenario. Concluding remarks are found in Section 4.

2. Methodology

Energy storage models have been widely developed for a variety of economic applications, optimal control, and system sizing. In this section, an ERM is described along with the economic structure of a peak shaving scenario. ERMs describe the system in terms of energy flow between battery, generation, and load. These are the simplest models, but well suited for economic studies [25]. Fig. 1 shows the iterative method proposed in this paper as a flow chart.

This method is devised such that the optimization model is exchangeable so long as there is a charge and discharge profile of the BESS as an output and HVAC power as an input. Similarly, so long as there is a suitable location for the BESS any EnergyPlus input file is usable. The location will determine weather data and rate structure. Battery type will determine the battery model used to calculate heat loss from battery to enclosure. PCS placed inside or outside the enclosure will determine whether to include PCS inefficiency in the heat balance. PYOMO and EnergyPlus models are created for the optimization and heat balance respectively. Sections 2.1 and 2.2 define the PYOMO model, while Sections 2.3 and 2.4 define the EnergyPlus model. The PYOMO sizing model is first solved with no consideration for the HVAC load to provide the BASE solution. The charge–discharge profile is taken from the BASE solution and used in an EnergyPlus simulation, which solves for the HVAC load that is used to update the PYOMO model. Convergence is not guaranteed as the relationship between BESS parameters and HVAC load solution is nonlinear and non-convex. Therefore, the process is repeated until both the energy capacity and power rating of the BESS meet convergence criteria or a maximum number of iterations are run. However, in Fig. 2 the BESS parameters are seen to rapidly converge in the first few iterations. This provides the minimum sized BESS to provide the service required at a certain location.

2.1. Linear energy reservoir model

The ERM assumes a linear relationship between system power and stored energy. As the ERM is affine, it is widely used in convex economic optimization problems [30] and is formulated as follows:

$$S_i = n^s S_{i-1} + n^{\mathrm{rt}} \tau p_i^c - \tau p_i^d, \forall i \in \mathbf{A} \quad (1)$$

where S_i is the state of energy (MWh) at the ith timestep of length τ (hr). The storage efficiency n^s and round trip efficiency n^{rt} are assumed constant while the charge power p^c (MW) and discharge power p^d (MW) are the average value over the time step and defined to be nonnegative. The ESS device is also constrained by

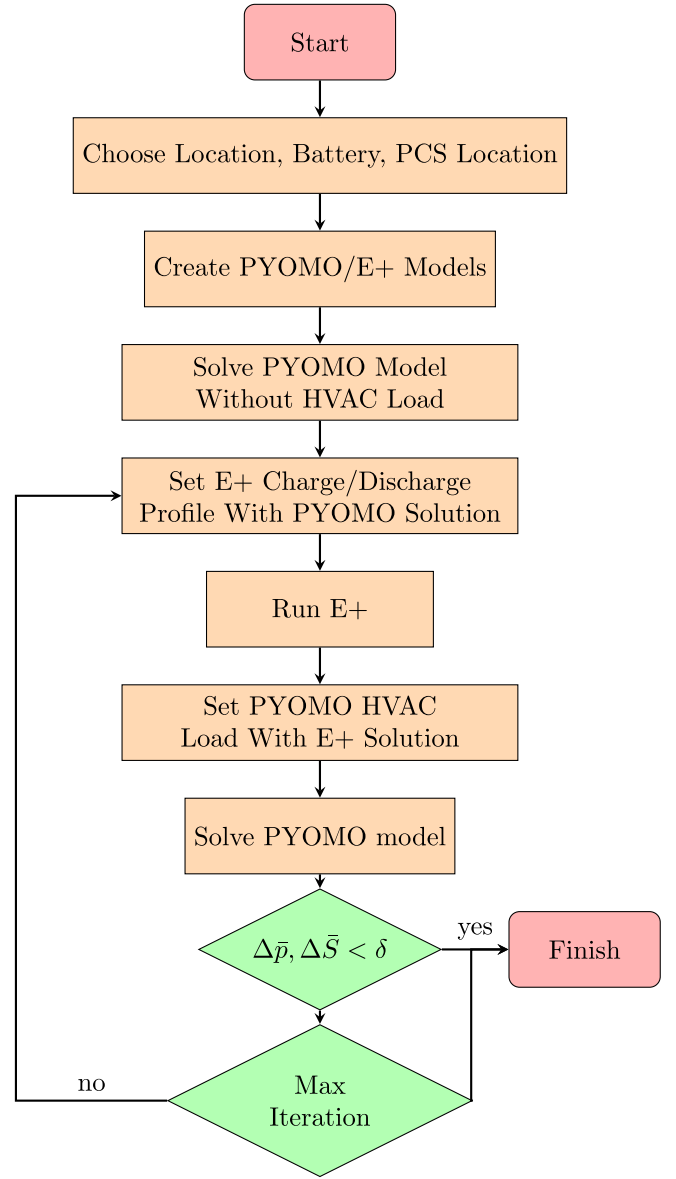$$0 \leq q_i^c + q_i^d \leq Q, \forall i \in \mathbf{A} \quad (2a)$$

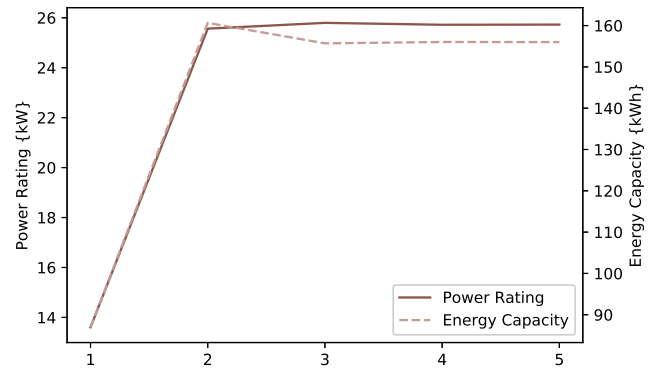**Fig. 1.** Iterative solution flow chart.

Fig. 2. Power Rating and Energy Capacity of BESS in Minneapolis, MN, at each iteration. The values converge quickly at the fifth iteration.

$$S_{\min} \leq S_i \leq S_{\max}, \forall i \in \mathbf{A} \quad (2b)$$

$$\sum_{i \in A} n^{rt} q_i^c - q_i^d = 0. \tag{2c}$$

where the equivalent energy terms, τp, have been replaced with energy variables q. The constraint (2a) ensures charge and discharge profile is within the capabilities of the ESS. The constraint (2b) requires the state of charge of the system to be within a specified minimum and maximum amount. The constraint (2c) requires the net charging to be zero, or the initial and final state of charge (SOC) to be equal. The complimentary slackness constraint is not included because it is assumed any simultaneous charging and discharging would be settled within the time period.

2.2. Battery energy storage system sizing problem formulation

The optimization seeks to minimize the BESS cost and the energy bill. The BESS capital cost is proportional to the energy capacity and power rating. The energy bill is calculated using the utility rate structure for a particular location. A simple rate structure may have a flat rate energy charge the entire year, while time of use (TOU) rate structures may have energy charges that vary by hour, day, and season. Customers may also have a demand charge per kW of the highest power consumption for a specified duration, typically 15 min. These demand charges may also vary by hour, day, and season. Rates are set in advance and are not subject to change during the contract period. Higher energy and demand rates during peak time periods offer customers the incentive to decrease consumption at times of high load allowing utilities to manage their total peak loads. However, these customers must have the ability to reduce or shift their load. While it may be possible to reduce consumption in peak times for residential customers, often commercial and industrial customers do not have that flexibility. Energy storage devices offer a solution to that problem by discharging during peak periods and charging in the off peak periods. This demand response strategy saves the customer money, while helping the utility manage their peak load. The cost minimization problem can be formulated as a LP [31]:

$$\min\{C^{BESS} + C^E\} \tag{3a}$$

$$s.t \quad (1), (2a), (2b), (2c),$$

$$q_i^d + q_i^{\text{grid}} - q_i^c = q_i^{\text{load}} + q_i^{\text{hvac}}, \forall i \in \mathbf{A} \tag{3b}$$

$$q_i^c + q_i^{\text{grid}} \le q^{\max}, \forall i \in \mathbf{A} \tag{3c}$$

where,

$$C^{ESS} = c^p \bar{p} + c^q \bar{S} \tag{3d}$$

$$C^E = \sum_{m \in \mathbf{M}} (q^{\max} c_m^d + \sum_{i \in \mathbf{A}_m} (q_i^{\text{grid}} + q_i^c) c_m^e). \tag{3e}$$

where C^{BESS} and C^E are the capital costs of the BESS and cost of electricity. The excess energy bought from the grid, energy consumed by the load, and energy consumed by the HVAC device are represented by q_i^{grid} q_i^c q_i^{load}, and q_i^{hvac}, respectively. The maximum allowable energy to be drawn from the grid in each time step is represented by q_{max}. The power rating and energy capacity of the BESS is represented by $\bar{p}$ and $\bar{S}$. The capital cost per kW is represented by c^p, while the capital cost per kWh is represented by c^q. The demand charge of each month is represented by c_m^d and the electricity cost of each month is represented by c_m^e. $\mathbf{M}$ is the set containing all months of the year while $\mathbf{A_m}$ is the set containing all time steps within the month m. The constraint (3b) requires that there be enough energy between the grid and ESS to provide for the load and HVAC energies. The constraint (3c) limits the energy drawn from the grid at each time step, i, within the time period below the maximum value, i.e. the peak load constraint. Then, the above problem seeks to minimize the capital cost of the ESS along with the energy bill for a peak shaving scenario. This approach assumes perfect foresight and thus gives the best case solution.

Table 1
Characteristics of shipping container materials.

Property	Corten steel [35]	Marine plywood	Steel
Roughness	MediumRough	Smooth	Smooth
Thickness {m}	0.002	0.028	0.127
Conductivity {$\frac{W}{mK}$}	16.00	0.12	45.28
Density {$\frac{kg}{m^3}$}	8000	540	7824
Specific heat {$\frac{J}{kgK}$}	500	1210	500
Thermal absorptance	0.89	–	–
Solar absorptance	0.913	–	–

Table 2
Specifications of packaged terminal air conditioning unit.

Property	Rating
Fan Placement	Draw Through
Fan Efficiency	70%
Fan Pressure Difference	75 Pa
Fan Motor Efficiency	90%
Cooling Coil Rated Capacity	15000 W
Cooling Coil Coefficient of Performance	3
Heating Coil Rated Capacity	25000 W
Heating Coil Efficiency	100%

2.3. Energy plus

Energy Plus is a building simulation software used to model energy consumption developed by the US Department of Energy's Building Technology Office and first released in April of 2001. The software has been widely adopted as a leader in building energy simulation. EnergyPlus is a console-based program that can be run from the command line with specified input files. Comprehensive graphical interfaces are available along with the software development kit OpenStudio [32]. In release 9.3 [28], EnergyPlus was updated with an application programming interface (API) that allows users to write scripts in C or Python to run and manipulate EnergyPlus simulations. The inner workings of EnergyPlus have been well documented and the readers are directed [28, 29,33,34] for more information. The following is an explanation of the features important to the work presented.

The Energy Plus input file (IDF) contains all of the details pertaining to the building's energy and mass transfer. Many options are available [34], however a simple description of the BESS enclosure is presented. Typically, standalone battery energy storage devices are housed in shipping containers. Standard high cube units are constructed with lengths of 10', 20', and 40', with a standard width and height of 8' × 9'6". The walls and doors consist of a 2 mm layer corten steel while the floor is a 28 mm layer of marine plywood fastened on top of steel crossbars [35]. The relevant characteristics of each material is listed in Table 1. The roughness property corresponds to a keyword in Energy Plus related to convection coefficient calculations [34]. Thermal and solar absorptance are ratios and default values are used where the information could not be found.

HVAC units are compound objects built with individually modeled components in EnergyPlus. The complete objects in EnergyPlus become very complex to create in the IDF, however HVAC Template objects allow for more simple design choices such as heating or cooling capacity while the basic layout of the HVAC is already packaged. For this study, a packaged terminal air conditioner (PTAC) is modeled within the shipping container enclosure.

The PTAC is a single unit, similar to what may be placed under the window in a hotel room, with both heating and cooling capabilities. Outside air is mixed with the exhaust air, which is blown through the heating or cooling elements to provide conditioned air to the space. The configuration consists of an outdoor air mixer, electric heating coil, direct expansion cooling coil, and fan. Design specifications are listed in Table 2.

Table 3
LG 18650 characteristics [38,39].

Chemistry	NMC
$\bar{q}$	2.5 Ah
$\bar{v}$	3.6 V
r	0.02 Ω
k	0.005 Ω
Temperature range	15–40 °C

Table 4
Location climate zones [40].

Location	AKA	AKF	CO	MA	MN	MT	ND	NY
Climate zone	7	8	7	5	6	6	6	5

2.4. Non-linear energy reservoir model

A technology specific non-linear energy flow model proposed in [36] is used to describe the heat loss of the battery. Energy flow models, as used in the energy storage system model in Section 2.1, are well suited for techno-economic studies because they describe battery energy storage behavior over suitable time periods for market operation. Real batteries lose energy at rates that depend on the state of charge, temperature, and charge or discharge power [37] which makes the efficiency terms non-linear. The non-linear formulation of (1) is expressed as [36]:

$$S_i = n^s S_{i-1} + \tau f_i^c(p_i^c, S_{i-1}) - \tau f_i^d(p_i^d, S_{i-1}) \tag{4}$$

where f^c and f^d represent the average charged and discharged power over a time step, respectively. The rate of energy loss for Lead–acid and Li-ion batteries during charge and discharge can be characterized with system level quantities as [36]:

$$p_i^{ld} \approx \frac{\bar{q}}{\bar{v}\bar{S}}[(r + \frac{k\bar{S}}{S_i})(\frac{p_i^d}{n^p})^2 + \frac{k\bar{S}(\bar{S} - S_i)}{S_i}\frac{p_i^d}{n^p}] \tag{5}$$

$$p_i^{lc} \approx \frac{\bar{q}}{\bar{v}\bar{S}}[(r + \frac{k\bar{S}}{\bar{S} - S_i})(n^p p_i^c)^2 + \frac{k\bar{S}(\bar{S} - S_i)}{S_i}n^p p_i^c] \tag{6}$$

where $\bar{S}$ as the rated energy capacity of the system, $\bar{q}$ as the rated ampere-hour capacity of a battery cell, $\bar{v}$ as the rated voltage of a battery cell, r as the internal resistance of a battery cell, n^p as the power conversion system efficiency, and the model coefficient k can be calculated from nameplate or testing data [36]. Then the charged and discharged power at each time step is the sum of consumed power and power loss:

$$f_i^d = \frac{p_i^d}{n^p} + p_i^{ld} \tag{7}$$

$$f_i^c = n^p p_i^c - p_i^{lc} \tag{8}$$

The energy lost as heat to the enclosure is given by the first terms in Eqs. (5) and (6) related to the ohmic and polarization resistances. Using the EnergyPlus API, the heat energy is released into the enclosure model using the Electric Equipment object [34].

A lithium nickel manganese cobalt oxide (NMC) battery is considered with characteristics shown in Table 3. For each location a scenario in which the PCS is considered to be inside the enclosure is also simulated, where the inefficiency is considered to be lost as heat. The enclosure temperature is kept between the operating range of each battery shown in Table 3.

3. Results

In this section, the results of running simulations for the eight locations shown in Table 4 are presented. A load profile representing a warehouse is used, accessible from [41] and shown in Fig. 3. All weather files are TMY3 available from the EnergyPlus website [28].

The cost of lithium ion batteries are estimated on a per kW (c^p), and per kWh (c^q) basis as described in (3d). These costs are determined using a regression algorithm on the data presented in [42] as 132.36 $\frac{\$}{kW}$ and 360.38 $\frac{\$}{kWh}$. The storage efficiency and round-trip efficiency of (1) are 100% and 83.32%, respectively, while the PCS efficiency is 93.32%.

S_{min} and S_{max} are set to 5% and 95% of battery capacity due to the asymptotic relationship between power loss and charging when the battery is near a full charge or discharging when near fully discharged. In the former case battery voltage is high due to low current, while the opposite is true in the latter. Both scenarios result in poor battery performance with high losses. This means $\bar{S}$ represents the cell-level capacity of the system while the operating range of the system is between S_{min} and S_{max}. Therefore, the AC nameplate capacity of the system is S_{max} minus S_{min}.

The peak shaving case studies presented assume the customer desires to limit the total load to 70 kW. The rate structure of AKF is used in each simulation, which has a constant energy charge of 0.12638 $\frac{\$}{kWh}$ and constant demand charge of 22.27 $\frac{\$}{kW}$ throughout the year [43].

Fig. 4 shows the resulting optimal battery sizes for each location and PCS heat loss scenario. The solution in which parasitic losses are not considered, BASE, is independent of location, shown at 86.9 kWh, 13.6 kW. This is because, by choice, the weather data and consequently the HVAC load is the only variation between simulations, isolating the climate effects.

The results vary significantly between locations and whether the PCS is considered to be contained in the enclosure. AKF, residing in the subarctic thermal climate zone, nearly triples the required energy capacity and power rating of the battery to 261.6 kWh, 29.6 kW with PCS outside of the enclosure. When PCS is considered inside of the enclosure the sizes are reduced to 220.1 kWh, 28.4 kW. MT has the smallest optimal battery sizes at 131.4 kWh, 21.8 kW with PCS outside the enclosure and 123.7 kWh, 21.2 kW with PCS inside the enclosure.

The results show large differences between locations in the same climate zone designation. AKF, the only location in climate zone 8, requires the largest BESS. AKA and CO, both residing in climate zone 7, differ by roughly 30 kWh, 1 kW with PCS both inside and outside. ND, MN, and MT all are classified in climate zone 6, however ND requires the second largest BESS while MT requires the smallest optimal BESS. The two locations in climate zone 5, NY and MA, differ by 10 kWh with PCS outside and 10 kWh, 1 kW with PCS inside the enclosure.

Optimal BESS sizes vary by the climate location, but are also dependent on the load profile shown in Fig. 3. The load consistently peaks during weekdays to 83 kW in January, November, and December while the rest of the year has peaks of 74 kW. The BESS size will then depend on HVAC consumption during these peak winter months.

Fig. 5 shows the daily battery usage, enclosure HVAC consumption, and mean outdoor air temperature during the peak winter months in the three extreme locations by climate zone AKF, AKA, and CO, with the addition of ND since it has the second largest size. Cold temperatures drive HVAC consumption, which in turn drives the battery usage. AKF has extended periods of extremely low temperatures driving high HVAC consumption and battery usage during weekdays. AKA and ND, while not as extreme, also have periods of low temperatures and high HVAC consumption during the first weeks of January and December. ND particularly, peaks nearly as high as AKF in HVAC consumption in January, however this falls on the weekend when the load is low therefore the battery is not in use. CO has the least extreme temperatures and HVAC consumption displayed, resulting in the least battery usage. While not displayed in the figure, similar results are obtained for the other four locations.

Parasitic HVAC loads of the enclosure affect the amount of battery energy able to be used toward the load. Fig. 6 shows the percent of charged battery energy used to power the load and Fig. 7 shows the percent used toward heating and cooling the BESS enclosure. In each location these parasitic loads require a significant amount of
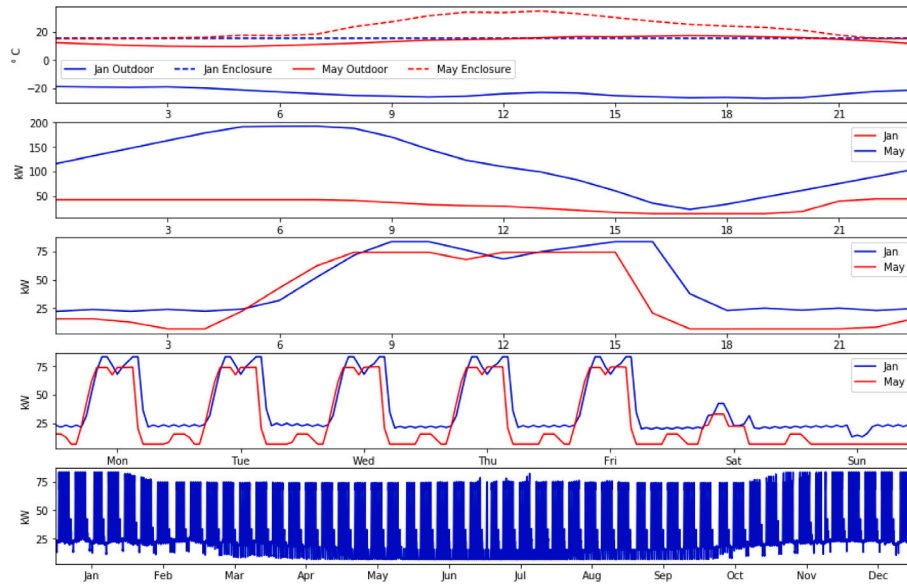
Fig. 3. From top to bottom: outdoor and enclosure temperature of January 3rd and June 6th, battery SOC of January 3rd and June 6th, hourly load of January 3rd and June 6th, hourly load of January 3–9 and June 5–11, and hourly load of the entire year.
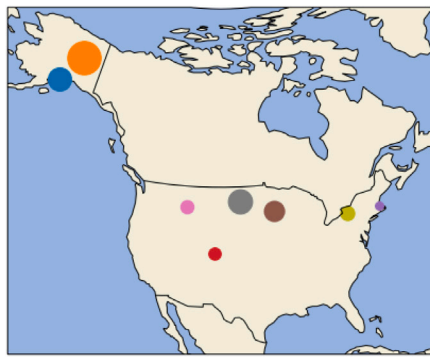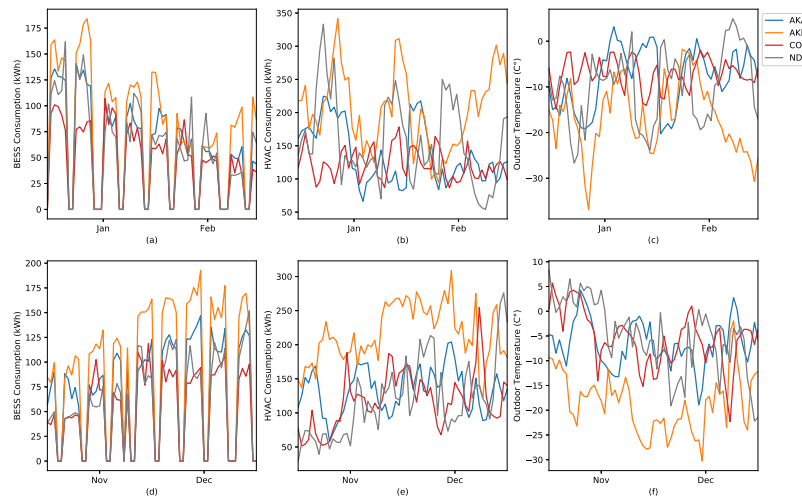

(a) BESS energy capacity sizes when PCS is outside the enclosure on map of North America.
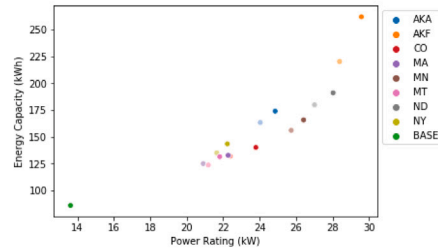
(b) Optimal power rating and energy capacity. The light shaded colors indicate the PCS inside the enclosure, while the darker shade indicates PCS outside the enclosure.

Fig. 4. Optimal BESS sizes in each location.

Fig. 5. Battery usage during peak winter months in AKF, AKA, CO, and ND with PCS inside the enclosure. (a) and (d) daily energy usage of BESS, (b) and (e) daily enclosure HVAC energy consumption, (c) and (f) daily mean temperature. (a), (b), and (c) span January and February while (d), (e), and (f) span November and December.
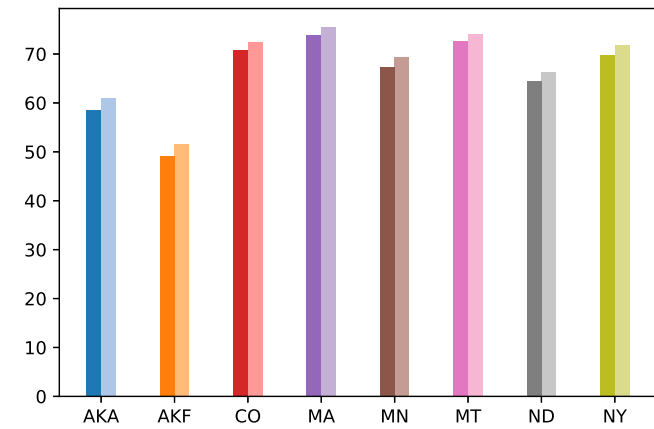
Fig. 6. The percent of energy charged by the battery consumed by the load. The light shaded colors indicate the PCS inside the enclosure, while the darker shade indicates PCS outside the enclosure.
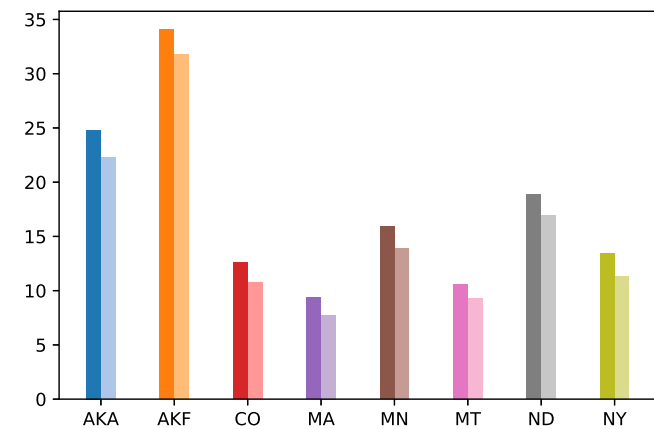

Fig. 7. The percent of energy charged by the battery consumed by the enclosure HVAC. The light shaded colors indicate the PCS inside the enclosure, while the darker shade indicates PCS outside the enclosure.

Fig. 8. Optimal BESS cost in each location. The light shaded colors indicate the PCS inside the enclosure, while the darker shade indicates PCS outside the enclosure. The green horizontal line represents the BASE BESS capital cost at $33,137.

Fig. 9. Annual energy bill at each location relative to the case without BESS. A negative relative bill indicates saving money while a positive relative bill indicates a more expensive bill. The light shaded colors indicate the PCS inside the enclosure, while the darker shade indicates PCS outside the enclosure.

battery energy from 8% in MA with PCS inside the enclosure to 34% in AKF with PCS outside the enclosure. In the extreme case of AKF, this reduces the amount of energy used toward the load to 49%. Placing PCS inside the enclosure reduces the usage of energy toward the HVAC by roughly 2% in each location. The percent of battery energy used toward parasitic loads corresponds to relative optimal battery sizes with the exception of AKA which has the second largest portion of battery energy consumed by the enclosure HVAC load, while having the third largest battery size.

Fig. 8 shows the capital cost of the optimal BESS in each location. Since the cost of energy capacity is higher and the power ratings have less variation, the cost among locations follows the energy capacity size. The savings associated with having PCS inside the enclosure is also higher as the battery size is larger. AKF with PCS outside the enclosure is the most expensive battery at $98,211. Placing PCS inside the enclosure reduces capital cost of the battery to $83,061 saving $15,150.

Fig. 9 shows the change in the expected energy bill from installation of the optimal BESS. The BASE solution predicts $659 of savings, highlighting that peak shaving is not a financially viable use case for energy storage in itself. Including the parasitic HVAC losses in the solution increases the energy bill in each case. AKF has the largest increase, paying an excess bill of $5,104 when PCS is inside the enclosure and $5,479 when PCS is outside the enclosure. AKA, ND, and CO follow with about half the relative utility bill of AKF, while the more mild climates of NY and MA have a smaller increase in bill. Given that each
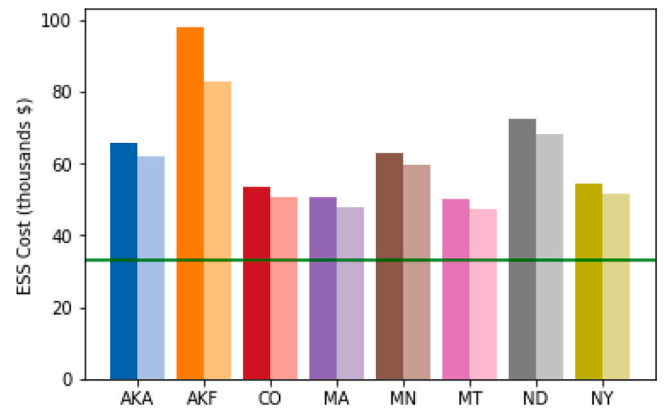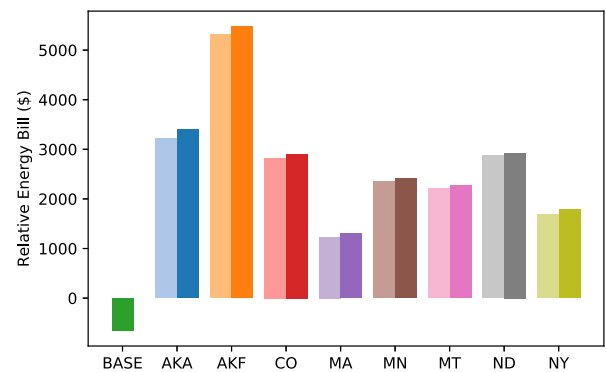
location has the same rate structure in the simulations, the increase in energy bill is attributed to the increased HVAC usage due to the extremity of the climate. Thus, without considering heating and cooling loads a BESS owner would have thought they would save money, when in fact they would have paid at least a thousand more in each case.

These results show that locations with extreme cold climates are the most affected in terms of battery size, resulting in more expensive capital costs and energy bills. The regional climate zone as defined in [40] did not directly predict relative battery size in each location. AKF has the most extreme climate resulting in the largest BESS and costs, however the next largest BESS was located in ND which is in climate zone 6. The optimal BESS in CO, in climate zone 7, is among the lowest in sizes. This supports the usefulness of the method presented in this study as the local climate strongly impacts BESS sizes. TMY3 files contain representative annual weather data for a location useful for comparative results. However, they will not capture all of the extremities associated with each location, in which a stochastic study may provide more insight.

Topics not considered in this study include varying the load profile, rate structure, use case, and enclosure. The load profile has an impact on BESS sizes, however a similar locational dependence would be expected for other cases. Insulating the shipping container or considering different building enclosures may enhance thermal management and provide advantages not considered in this study. Using local rate structures adds further complexity and may only significantly alter the results when the BESS heat loss and HVAC consumption are comparable, in which case the BESS operation will affect when the largest

parasitic loads occur. Different use cases of the BESS would likely affect the overall economics and would be interesting future work, however it is beyond the scope of this paper.

4. Conclusion

The effects of parasitic heating and cooling loads on BESS sizing are investigated in this paper. Sizing problems are formulated for the peak shaving case as a linear program with the PYOMO python package. HVAC loads are incorporated using EnergyPlus to model a BESS enclosure, namely a shipping container with a PTAC unit in eight U.S. locations considering an NMC lithium-ion battery type and whether the PCS is inside or outside the enclosure.

Results show that locations with extreme winters, such as Fairbanks, AK, require a significantly larger battery capacity than would be anticipated without considering parasitic HVAC loads. Given that all operating conditions are kept constant besides the local climate, Fig. 5 illustrates this point. The locations with the largest required battery size, AKF and ND, have the coldest winter months driving higher HVAC consumption. The BESS is then required to provide more energy to keep the total load under the prescribed 70 kW. However, even the case with the smallest resulting battery sizes, MT with PCS inside the enclosure, requires an increase of 42% in energy capacity, 56% in power rating, and 43% in the capital cost as compared to the BESS models currently used in techno-economic studies. Placing the PCS inside the BESS enclosure results in savings of roughly 6% on capital costs in every location except AKF where the savings are roughly 18%. While predicting a modest return in annual energy bill savings in the BASE case, Fig. 9 shows the increase in energy bill due to the HVAC loads costs the end user more money in each case. This result is not unexpected, but can be improved upon with model predictive control methods [25].

These results suggest that HVAC loads have a significant effect and warrant consideration in techno-economic studies. Future applications of this work would consider different built enclosures and HVAC technologies, off-grid sizing, economic use cases, and thermal management schemes.

CRediT authorship contribution statement

Walker Olis: Conceptualization, Methodology, Software, Writing – original draft. **David Rosewater:** Conceptualization, Methodology, Validation, Writing – review & editing. **Tu Nguyen:** Conceptualization, Methodology, Writing – review & editing. **Raymond H. Byrne:** Conceptualization, Supervision, Writing – review & editing.

Declaration of competing interest

The authors declare that they have no known competing financial interests or personal relationships that could have appeared to influence the work reported in this paper.

Data availability

Data will be made available on request.

Acknowledgments

References

[1] Bayindir R, Hossain E, Vadi S. The path of the smart grid -the new and improved power grid. In: 2016 International smart grid workshop and certificate program. 2016, p. 1–8. http://dx.doi.org/10.1109/ISGWCP.2016.7548270.

[2] Tian Y, Bera A, Benidris M, Mitra J. Reliability and environmental benefits of energy storage systems in firming up wind generation. In: 2017 North American power symposium. 2017, p. 1–6. http://dx.doi.org/10.1109/NAPS.2017.8107315.

[3] Alizadeh M, Parsa Moghaddam M, Amjady N, Siano P, Sheikh-El-Eslami M. Flexibility in future power systems with high renewable penetration: A review. Renew Sustain Energy Rev 2016;57:1186–93. http://dx.doi.org/10.1016/j.rser.2015.12.200, URL https://www.sciencedirect.com/science/article/pii/S136403211501583X.

[4] Eyer J, Corey G. Energy storage for the electricity grid: Benefits and market potential assessment guide. Tech. rep. SAND2010-0815, Albuquerque, NM: Sandia National Laboratories; 2010.

[5] Oh S, Kong J, Lee W, Jung J. Development of optimal energy storage system sizing algorithm for photovoltaic supplier in South Korea. In: 2018 IEEE power energy society general meeting. 2018, p. 1–5. http://dx.doi.org/10.1109/PESGM.2018.8586289.

[6] Yoo Y, Jang G, Jung S. A study on sizing of substation for PV with optimized operation of BESS. IEEE Access 2020;8:214577–85. http://dx.doi.org/10.1109/ACCESS.2020.3040646.

[7] Narimani MR, Asghari B, Sharma R. Optimal sizing and operation of energy storage for demand charge management and PV utilization. In: 2018 IEEE/PES transmission and distribution conference and exposition. 2018, p. 1–5. http://dx.doi.org/10.1109/TDC.2018.8440302.

[8] Moghaddam IN, Chowdhury B. Optimal sizing of hybrid energy storage systems to mitigate wind power fluctuations. In: 2016 IEEE power and energy society general meeting. 2016, p. 1–5. http://dx.doi.org/10.1109/PESGM.2016.7741862.

[9] Alsaidan I, Khodaei A, Gao W. A comprehensive battery energy storage optimal sizing model for microgrid applications. IEEE Trans Power Syst 2018;33(4):3968–80. http://dx.doi.org/10.1109/TPWRS.2017.2769639.

[10] Alharbi AM, Gao W, Alsaidan I. Sizing battery energy storage systems for microgrid participating in ancillary services. In: 2019 North American power symposium. 2019, p. 1–5. http://dx.doi.org/10.1109/NAPS46351.2019.9000306.

[11] Hassan A, Al-Abdeli YM, Masek M, Bass O. Optimal sizing and energy scheduling of grid-supplemented solar pv systems with battery storage: Sensitivity of reliability and financial constraints. Energy 2022;238:121780. http://dx.doi.org/10.1016/j.energy.2021.121780, URL https://www.sciencedirect.com/science/article/pii/S0360544221020284.

[12] Chennaif M, Zahboune H, Elhafyani M, Zouggar S. Electric system cascade extended analysis for optimal sizing of an autonomous hybrid CSP/PV/wind system with battery energy storage system and thermal energy storage. Energy 2021;227:120444. http://dx.doi.org/10.1016/j.energy.2021.120444, URL https://www.sciencedirect.com/science/article/pii/S0360544221006939.

[13] Gul E, Baldinelli G, Bartocci P, Bianchi F, Domenghini P, Cotana F, et al. A techno-economic analysis of a solar PV and DC battery storage system for a community energy sharing. Energy 2022;244:123191. http://dx.doi.org/10.1016/j.energy.2022.123191, URL https://www.sciencedirect.com/science/article/pii/S0360544222000949.

[14] Khaki B. Joint sizing and placement of battery energy storage systems and wind turbines considering reactive power support of the system. J Energy Storage 2021;35:102264. http://dx.doi.org/10.1016/j.est.2021.102264, URL https://www.sciencedirect.com/science/article/pii/S2352152X21000311.

[15] Xie C, Wang D, Lai CS, Wu R, Wu X, Lai LL. Optimal sizing of battery energy storage system in smart microgrid considering virtual energy storage system and high photovoltaic penetration. J Clean Prod 2021;281:125308. http://dx.doi.org/10.1016/j.jclepro.2020.125308, URL https://www.sciencedirect.com/science/article/pii/S0959652620353531.

[16] Liu Y, Wu X, Du J, Song Z, Wu G. Optimal sizing of a wind-energy storage system considering battery life. Renew Energy 2020;147:2470–83. http://dx.doi.org/10.1016/j.renene.2019.09.123, URL https://www.sciencedirect.com/science/article/pii/S096014811931465X.

[17] He Y, Guo S, Zhou J, Song G, Kurban A, Wang H. The multi-stage framework for optimal sizing and operation of hybrid electrical-thermal energy storage system. Energy 2022;245:123248. http://dx.doi.org/10.1016/j.energy.2022.123248, URL https://www.sciencedirect.com/science/article/pii/S0360544222001517.

[18] Zolfaghari M, Ghaffarzadeh N, Ardakani AJ. Optimal sizing of battery energy storage systems in off-grid micro grids using convex optimization. J Energy Storage 2019;23:44–56. http://dx.doi.org/10.1016/j.est.2019.02.027, URL https://www.sciencedirect.com/science/article/pii/S2352152X18308120.

[19] Yuan Z, Wang W, Wang H, Yildizbasi A. A new methodology for optimal location and sizing of battery energy storage system in distribution networks for loss reduction. J Energy Storage 2020;29:101368. http://dx.doi.org/10.1016/j.est.2020.101368, URL https://www.sciencedirect.com/science/article/pii/S2352152X20301286.

[20] Singh A, Nguyen HD. A two-layer framework for optimal control of battery temperature and microgrid operation. J Energy Storage 2022;50:104057. http://dx.doi.org/10.1016/j.est.2022.104057, URL https://www.sciencedirect.com/science/article/pii/S2352152X22000949.

[21] Xiong B, Yang Y, Tang J, Li Y, Wei Z, Su Y, et al. An enhanced equivalent circuit model of vanadium redox flow battery energy storage systems considering thermal effects. IEEE Access 2019;7:162297–308. http://dx.doi.org/10.1109/ACCESS.2019.2952212.

[22] Ma Y, Ding H, Liu Y, Gao J. Battery thermal management of intelligent-connected electric vehicles at low temperature based on NMPC. Energy 2022;244:122571. http://dx.doi.org/10.1016/j.energy.2021.122571, URL https://www.sciencedirect.com/science/article/pii/S0360544221028206.

[23] Wang Y, Zhou C, Chen Z. Optimization of battery charging strategy based on nonlinear model predictive control. Energy 2022;241:122877. http://dx.doi.org/10.1016/j.energy.2021.122877, URL https://www.sciencedirect.com/science/article/pii/S0360544221031261.

[24] Hu X, Liu W, Lin X, Xie Y. A comparative study of control-oriented thermal models for cylindrical Li-Ion batteries. IEEE Trans Transp Electr 2019;5(4):1237–53. http://dx.doi.org/10.1109/TTE.2019.2953606.

[25] Rosewater DM, Copp DA, Nguyen TA, Byrne RH, Santoso S. Battery energy storage models for optimal control. IEEE Access 2019;7:178357–91. http://dx.doi.org/10.1109/ACCESS.2019.2957698.

[26] Hart WE, Watson J-P, Woodruff DL. Pyomo: modeling and solving mathematical programs in Python. Math Program Comput 2011;3(3):219–60.

[27] Hart WE, Laird CD, Watson J-P, Woodruff DL, Hackebeil GA, Nicholson BL, et al. Pyomo–optimization modeling in Python, vol. 67. 2nd ed. Springer Science & Business Media; 2017.

[28] US Department of Energy. Energy plus building simulation software. 2020, URL https://energyplus.net/.

[29] Crawley D, Pedersen C, Lawrie L, Winkelmann F. EnergyPlus: Energy simulation program. Ashrae J 2000;42:49–56.

[30] Mokrian P, Stephen M. A stochastic programming framework for the valuation of electricity storage. In: Proceedings 26th USAEE/IAEE North American conference. 2006, p. 24–7.

[31] Nguyen TA, Byrne RH. Maximizing the cost-savings for time-of-use and net-metering customers using behind-the-meter energy storage systems. In: 2017 North American power symposium. 2017, p. 1–6. http://dx.doi.org/10.1109/NAPS.2017.8107380.

[32] Guglielmetti R, Macumber D, Long N. OpenStudio: An open source integrated analysis platform; preprint. In: Proceedings of building simulation 2011: 12th Conference of international building performance simulation association. 2011.

[33] Crawley D, Lawrie L, Winkelmann F, Pedersen C. EnergyPlus: A new-generation building energy simulation program. In: Proceedings of FORUM 2001: Solar energy: The power to choose. American Solar Energy Society; 2001.

[34] Energy Plus Development Team. Energy plus version 9.4 documentation: Input output reference. 2020, URL https://energyplus.net/sites/all/modules/custom/nrel_custom/pdfs/pdfs_v9.4.0/InputOutputReference.pdf.

[35] Elrayies G. Thermal performance assessment of shipping container architecture in hot and humid climates. Int J Adv Sci Eng Inf Technol 2017;7:1114. http://dx.doi.org/10.18517/ijaseit.7.4.2235.

[36] Nguyen TA, Copp DA, Byrne RH, Chalamala BR. Market evaluation of energy storage systems incorporating technology-specific nonlinear models. IEEE Trans Power Syst 2019;34(5):3706–15. http://dx.doi.org/10.1109/TPWRS.2019.2909764.

[37] Nguyen TA, Crow ML. Stochastic optimization of renewable-based microgrid operation incorporating battery operating cost. IEEE Trans Power Syst 2016;31(3):2289–96. http://dx.doi.org/10.1109/TPWRS.2015.2455491.

[38] Technical Information of LG 18650HE2, URL https://www.powerstream.com/p/LG%2018650HE2%20Technical%20Information.pdf.

[39] IEEE/ASHRAE 1635-2018. 2018.

[40] Baechler MC, Gilbride TL, Cole PC, Hefty MG, Ruiz K. Building America best practices series volume 7.3: Guide to determining climate regions by county. Pacific Northwest National Laboratories; 2015.

[41] Commercial and residential hourly load profiles for all TMY3 locations in the United States, URL https://openei.org/datasets/files/961/pub/COMMERCIAL_LOAD_DATA_E_PLUS_OUTPUT/USA_AK_Fairbanks.Intl.AP.702610_TMY3/.

[42] Baxter R. 2019 Energy storage pricing survey. Tech. rep. SAND2021-0831, Albuquerque, NM: Sandia National Laboratories; 2021.

[43] Golden Valley Electric Association. GVEA rate schedules. 2021, URL https://www.gvea.com/rates/?doing_wp_cron=1612339564.1071701049804687500000.